Spin dynamics in the two-dimensional antiferromagnet La_2CuO_4

S. M. Hayden*
Institut Laue-Langevin, Boite Postale 156X, 38042 Grenoble CEDEX, France

G. Aeppli*
AT&T Bell Laboratories, Murray Hill, New Jersey 07974

H. A. Mook
Oak Ridge National Laboratory, Oak Ridge, Tennessee 37835

S-W. Cheong† and Z. Fisk
Los Alamos National Laboratory, Los Alamos, New Mexico 87545
(Received 29 March 1990)

The magnetic dynamics of La_2CuO_4 have been studied by means of inelastic neutron scattering in the energy range $0 \leq \hbar\omega \leq 140$ meV. Experiments were carried out using a wide range of incident neutron energies so as to optimize the experimental resolution in each energy range studied. For energy transfers, $\hbar\omega \geq 10$ meV, and temperatures T in the range $5 \leq T \leq 320$ K, we find that conventional spin-wave theory gives a good description of the magnetic dynamics. We obtain a low-temperature spin-wave velocity of $\hbar c$=850±30 meV Å. For low energies, $\hbar\omega \leq 10$ meV, and temperatures corresponding to the paramagnetic phase, our data indicate a response function consisting of overdamped spin waves and a quasielastic peak.

I. INTRODUCTION

Since the discovery of superconductivity in the doped CuO_2-based ceramics $La_{2-x}(Ba,Sr)_xCuO_4$ and $YBa_2Cu_3O_{6+\delta}$, the magnetic properties of the stoichiometric parent compounds have attracted considerable attention. However, the relationship between the antiferromagnetism present for some compositions and the superconductivity remains controversial. The magnetic correlations in these materials have been characterized by several microscopic techniques: light scattering,[1] muon spin relaxation,[2] and thermal neutron scattering.[3,4] Unfortunately, due to restrictions in range (for momentum and energy transfer) and resolution, the magnetic excitations near the zone center have not been characterized quantitatively. We report here a neutron-scattering study of the magnetic dynamics made over a range in energy transfer comparable to the intraplanar coupling constant. For our experiments we have used a wide variety of incident neutron energies (this was made possible by using "epithermal" and "cold" neutrons from special sources), thus optimizing the spectrometer resolution for each of the energy regimes studied.

The undoped compound La_2CuO_4 is a Mott insulator. There is a strong exchange coupling between the Cu^{2+} spins within the CuO_2 planes (see Fig. 1) and a weak coupling between spins in neighboring planes: the anisotropy of the coupling[5,6] is about 10^{-5}. This large anisotropy means that we have an excellent realization of a system with two-dimensional (2D) antiferromagnetic coupling. The weak coupling between spins in neighboring planes causes the system to order antiferromagnetically at about 300 K. The Néel temperature is very sensitive to doping, both by the substitution of Ba, Li, or Sr on the La sites and by the variation of the oxygen stoichiometry.[6]

Initial "energy-integrated" (the integration range extended to energy transfers with magnitude ~30 meV)

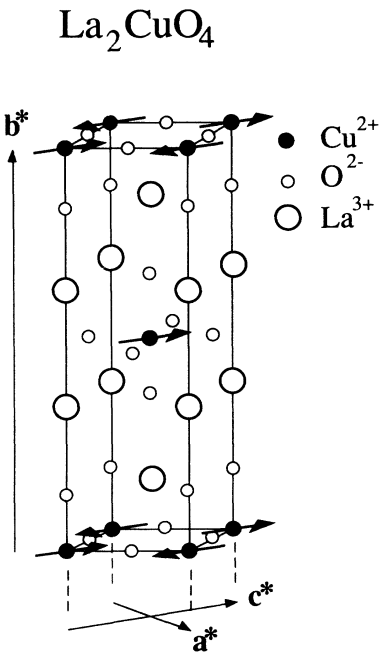

FIG. 1. Crystal structure of La_2CuO_4.

neutron-scattering investigations showed that La_2CuO_4 exhibits strong 2D magnetic correlations over a wide range in temperature.[3,7] The data were consistent with the scattering being strong along rods in reciprocal space, as would be expected for a 2D system. Inelastic neutron scattering revealed that the spin fluctuations had a large energy scale (>10 meV),[7,8] characteristic of a system with strong coupling between spins. However, experiments performed with thermal neutrons were unable to resolve the spin-wave branches: they provided only a lower bound to the coupling constant. In our study, we were not restricted by the kinematic constraints of thermal neutron scattering, and we were thus able to resolve the branches at high-energy transfer.

II. PRELIMINARIES

It has been suggested that La_2CuO_4 in its *paramagnetic state* is a good model for the 2D spin-$\frac{1}{2}$ Heisenberg antiferromagnet[5] described by the Hamiltonian,

$$H = \sum_{i,j} J S_i S_j \ , \tag{1}$$

where the sum is over nearest-neighbor spins in the same CuO_2 plane. In an ideal 2D Heisenberg system, thermal fluctuations would destroy the long-range order at finite temperature. The disorder is characterized by a length scale ξ, the correlation length. For sufficiently large wave vectors (i.e., $q \gg \xi^{-1}$) sharp propagating modes should exist even in a magnetically disordered (paramagnetic) medium.[9] In the regime where $a^{-1} \gg q \gg \xi^{-1}$, the conventional cross section for the scattering of neutrons from antiferromagnetic spin waves may be written (in the absence of spin-wave damping) in the form[10]

$$\frac{d^2\sigma}{d\Omega\, dE'} = \frac{k_f}{k_i} A(\omega)[\ \delta(\omega - cq)\delta(\mathbf{Q} - \mathbf{q} - \mathbf{G}) + \delta(\omega + cq)\delta(\mathbf{Q} + \mathbf{q} - \mathbf{G})] \ , \tag{2}$$

where $\mathbf{k}_i$ and $\mathbf{k}_f$ are the initial and final neutron wave vectors, respectively, and the scattering vector and the energy transfer are defined as $\mathbf{Q} = \mathbf{k}_i - \mathbf{k}_f$ and $\hbar\omega = E_i - E_f$, respectively. $\mathbf{G}$ is an antiferromagnetic reciprocal lattice vector and $A(\omega) \sim (1/\omega)(1 - e^{-\hbar\omega\beta})^{-1}$ contains a thermal population factor as well as the matrix element connecting the Néel state and a one-magnon state. We shall use the form (2) to analyze our high-energy measurements.

At low energies, $\hbar\omega \lesssim \hbar c\xi^{-1}$, we would expect collisions to cause the spin waves to be overdamped. This leads to a "quasielastic peak" for small wave vectors,[11] which would narrow with decreasing ξ^{-1} and turn into a magnetic Bragg peak if the system were to order two dimensionally. The magnetic excitation spectrum in this regime has recently been simulated by Tyč, Halperin, and Chakravarty (THC).[12] We can write the inelastic part of the differential cross section in the form,

$$\frac{d^2\sigma}{d\Omega\, dE'} = \sigma_0 \frac{k_f}{k_i} |f(\mathbf{Q})|^2 \frac{\chi''(\mathbf{q},\omega)}{1 - e^{-\hbar\omega\beta}} \ , \tag{3}$$

where $|f(\mathbf{Q})|$ is the magnetic form factor and $\chi(\mathbf{q},\omega)$ is the generalized spin susceptibility. For the case of spin waves with damping we will use the form

$$\chi''(q,\omega) = \frac{\chi(q)}{2}\left(\frac{\omega\Gamma_1}{\Gamma_1^2 + (\omega - cq)^2} + \frac{\omega\Gamma_1}{\Gamma_1^2 + (\omega + cq)^2}\right) \ , \tag{4}$$

where we have expanded the wave-vector-dependent susceptibility in the form $\chi(q) \sim (q^2 + \xi^{-2})^{-1}$. This was also the form used to fit the simulation results of THC.

III. EXPERIMENTAL

At high temperatures La_2CuO_4 has the K_2NiF_4 structure. It undergoes a tetragonal to orthorhombic distortion at about 530 K, which involves a staggered rotation of CuO_6 octahedra. Our crystals were grown from CuO-rich melts contained in a large Pt crucible (300 ml). High-purity powders of La_2O_3 and CuO were mixed in a stoichiometric ratio of La:Cu=1:2, heated above the peritectic melting temperature to (~1588 K), then slowly cooled down to the peritectic point ~1303 K, and finally quenched to room temperature. Crystals as large as $5 \times 5 \times 0.1$ cm^3 formed on the surface of the flux. After they were removed from the flux, the crystals were annealed at 1023 K under a flow of He gas and then furnace cooled to room temperature. Magnetic measurements on the crystals showed a sharp antiferromagnetic transition in the sense that the full width at half maximum (FWHM) of the susceptibility peak associated with the antiferromagnetic transition was ~13 K. The room-temperature lattice parameters (determined from x-ray diffraction) were a=5.375(2) Å, b=13.156(4) Å, and c=5.409(2) Å; note that throughout our work we follow previous practice and label points in reciprocal space using orthorhombic notation (see Fig. 1). The Néel temperature for our crystals varied from 260±5 to 290±5 K,

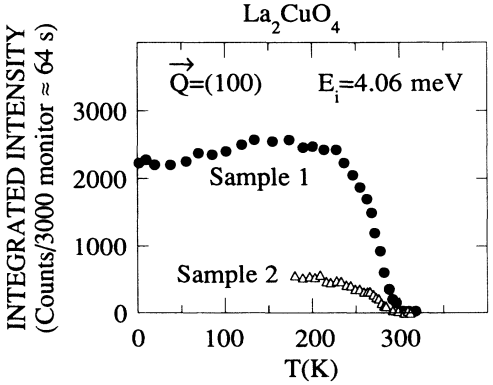

FIG. 2. The temperature dependence of the (100) magnetic Bragg peak intensity for two individual La_2CuO_4 crystals. The differing intensities are due to the use of different spectrometers and sample volumes.

with saturation of magnetic order for T<200 K. Figure 2 shows the variation of the (100) magnetic Bragg peak intensity for two of the crystals used. The sample used for the experiments at the highest-energy transfers consisted of an aligned array of 15 single crystals with a total volume of 8 cm^3. These crystals were aligned such that their in-plane axes coincided to better than 1.5°. At lower energies individual crystals were used. The crystals were mounted on either a room-temperature stage or on the cold finger of a ^{4}He cryostat. For the inelastic (triple-axis) and quasielastic (double-axis) measurements, the horizontal scattering planes of the instruments used coincided with the ($h0l$) and ($hk0$) [twinned with ($0kh$)] zones, respectively, of the crystals.

Measurements in the energy range $30 \leq \hbar\omega \leq 140$ meV were performed using IN1, the triple-axis spectrometer on the hot source at the Institut Laue-Langevin (ILL). In our experiments we used incident energies of up to 290 meV. A vertically curved copper (200) monochromator was used, with vertically curved graphite (002) or copper (200) crystals as analyzers. Curving the monochromator and analyzer allows a gain in signal at the expense of the out-of-plane resolution of the spectrometer. This is particularly useful here where the relaxed vertical resolution can be used to integrate along the **b*** direction in reciprocal space. Data were collected in two configurations: for lower-energy transfers we used the graphite (002) analyzer with a fixed final neutron energy, E_f=80 meV, at higher-energy transfers we used a copper (200) analyzer with E_f=150 meV. Higher-order contamination present from higher-order reflections at the monochromator was eliminated using nuclear resonance filters: a 0.4-mm-thick sheet of Er in front of the sample for E_f=80 meV or 0.5 mm of Hf before and 0.4 mm of Er after the sample for E_f=150 meV.

Triple-axis inelastic neutron-scattering data are usually collected as scans made as a function of momentum, q, or energy transfer $\hbar\omega$. If we wish to attempt to resolve two branches for a system with a steep dispersion such as La_2CuO_4, it is best to perform scans with constant energy transfer, $\hbar\omega$, as illustrated in Fig. 3. Resolution considerations mean that if the dispersion relation is linear, it is most favorable to work at high-energy transfers (and hence to use epithermal neutrons) to resolve the two branches. To arrive at the results presented in Figs. 4 and 6, we performed constant $\hbar\omega$ scans in the vicinity of the (100), (201), and (300) magnetic zone centers. As we increased the energy transfer, kinematic restrictions meant that it was necessary to increase the incident and final neutron energies as well as the length $|\mathbf{Q}|$ of the scattering vector. Each time the configuration was changed, scans were repeated at an energy transfer already measured, and the results used to cross calibrate. The scan directions were chosen to be optimal from resolution and background considerations. The energy and momentum resolutions (FWHM) were typically of order 10 meV and 0.05 $Å^{-1}$, respectively.

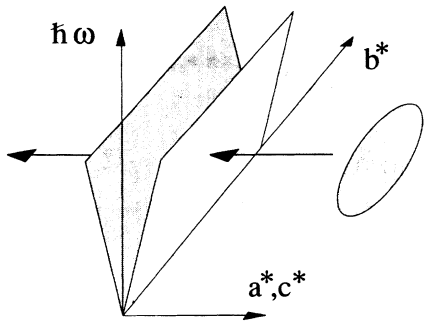

FIG. 3. Illustrates how constant energy scans were made through the spin-wave dispersion surface. The ellipsoid represents the instrumental resolution.

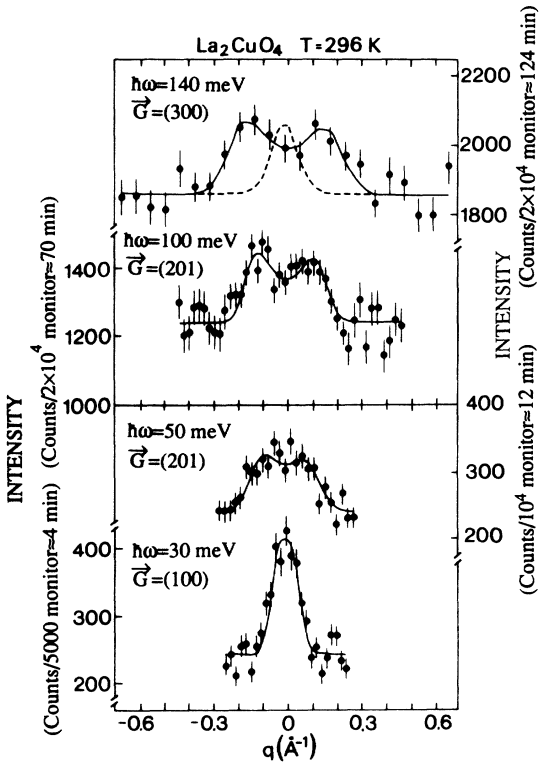

FIG. 4. IN1 (hot source, ILL) scans through the antiferromagnetic zone center for energy transfers $\hbar\omega$=30, 50, 100, and 140 meV. Due to kinematic restrictions, scans must be made under different conditions, thus the centers of the scans in momentum transfer were **G**=(100), (201), (201), and (300), respectively. The deviation of the scattering vector **Q** from **G** projected along (001) is q. The solid line represents a full resolution corrected fit of spin-wave theory to the data (see text). The dashed line in the upper frame corresponds to the resolution corrected cross section calculated for spin waves with infinite velocity for $\hbar\omega$=140 meV. The 30 and 50 meV scans were collected with a Cu(200) monochromator, a pyrolitic graphite (002) analyzer, and collimation of 25′-40′-20′-40′. The 100 and 140 meV scans were collected with a Cu(200) monochromator, a Cu(200) analyzer, and collimation of 25′-20′-40′-60′. Note that the 140-meV scan was performed on a sample volume of 8 cm^3; other scans were performed using a sample volume of 2 cm^3.

The thermal beam triple-axis spectrometer IN8 at the ILL was used to make measurements in the energy range $5 \leq \hbar\omega \leq 40$ meV. Vertically curved Cu(111) and Cu(220) monochromators were used with a vertically curved pyrolitic graphite (002) analyzer. A graphite filter was placed in the scattered beam, and a final energy of 14.7 meV was used. The monitor for the incident beam (used to determine the counting times) was corrected for higher-order contamination.

In order to characterize further the response at low energies, we performed high-resolution measurements on the cold-source triple-axis spectrometer TAS6 at Risø National Laboratory, Denmark. Here we used a vertically curved graphite (002) monochromator and analyzer. The final energy was fixed at 8.09 meV, with a graphite filter placed in the scattered beam. Under these conditions, constant $\hbar\omega$ scans performed in the manner described above are resolution limited. Thus we performed constant **q** scans. The energy resolution for $\hbar\omega = 0$ under these conditions is 0.5 meV (FWHM).

IV. RESULTS

Figure 4 shows IN1 (hot source) scans through the antiferromagnetic zone center for various energy transfers $\hbar\omega$. As $\hbar\omega$ increases, the scans become progressively wider. For the largest $\hbar\omega$ (≥ 0.1 eV), two maxima can be resolved in the scans. Figure 5 shows a series of longitudinal scans through the antiferromagnetic zone center at various energy transfers collected using the thermal-beam triple-axis spectrometer IN8. We note here the inability of thermal neutron scattering to resolve the spin-wave branches. The scans are, however, significantly broader than would be expected for spin waves of infinite velocity.

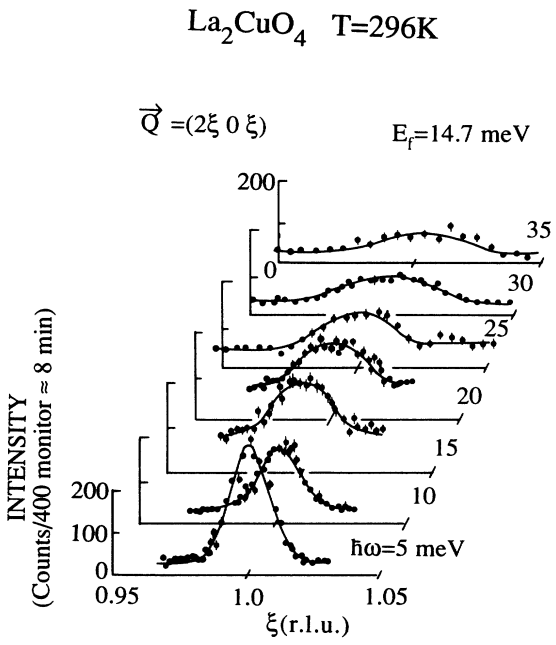

FIG. 5. IN8 (thermal beam, ILL) scans through the antiferromagnetic zone center (201). The solid lines are resolution corrected fits of spin-wave theory (see text). The $\hbar\omega$=5 and 10 meV scans were collected with monochromator, analyzer, and collimation of Cu(111)-PG(002) and 30′-20′-30′-40′, respectively; other scans were collected with Cu(220)-PG(002) and 30′-20′-40′-60′. The data shown in the figure have not been corrected for higher-order contamination in the incident beam: to correct for this the intensity of the 5 and 10 meV scans should be multiplied by 1.53 and 1.19, respectively. The sample volume was 8 cm^3.

The intensity distribution in our scans may be distorted by the instrumental resolution. For a nominal spectrometer setting $(\mathbf{Q}_0, \omega_0)$, the intensity is given by the convolution[13]

$$I(\mathbf{Q}_0,\omega_0) = A \int_{\Delta\mathbf{Q}} \int_{\Delta\omega} R(\mathbf{Q}-\mathbf{Q}_0, \omega-\omega_0) S(\mathbf{Q},\omega) d\omega d\mathbf{Q}, \tag{5}$$

where $R(\Delta\mathbf{Q}, \Delta\omega)$ is the instrumental resolution function[14] and the scattering law $S(\mathbf{Q},\omega)$ is defined by $d^2\sigma/d\Omega\, dE' = (k_f/k_i) S(\mathbf{Q},\omega)$. We analyze our data by choosing a model scattering law and fitting a convolution of this with the instrumental resolution function to the data, the integral (5) being performed numerically.

The solid lines in Figs. 4 and 5 represent fits of the simple cross section (2) for conventional spin waves to the data, while the dashed line in the top frame of Fig. 4 represents the calculated profile for an infinite spin-wave velocity. From the fits we can obtain the variation of the spin-wave propagation vector, $q_0 = \omega/c$, and the overall spin-wave amplitude, $A(\omega)$, with $\hbar\omega$: Figure 6 shows these results. For the energy range $10 \leq \hbar\omega \leq 140$ meV the energy dependence of the amplitude can be well described by conventional spin-wave theory, $A(\omega) \sim (1/\omega)(1 - e^{-\hbar\omega\beta})^{-1}$. The fitted pole positions are shown in Fig. 6, and the corresponding spin-wave velocities are $\hbar c$=850±30 meV Å and 750±30 meV Å for T=5 K and T=296 K, respectively.

In the low-energy regime, $\hbar\omega \leq 10$ meV in the paramagnetic phase, we performed measurements at T=320

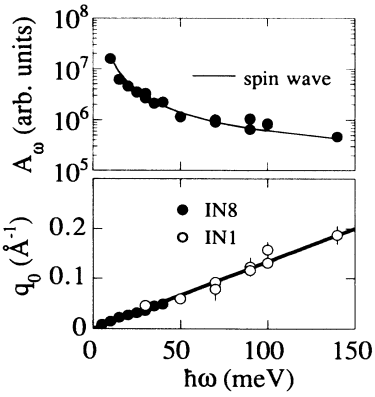

FIG. 6. Fitted spin-wave amplitudes (upper frame) and wave vectors (lower frame) obtained from constant energy scans for T=296 K.

K using a cold source triple-axis spectrometer. Figure 7(a) shows constant q scans on the rod and at a position nearby where no magnetic scattering is expected (as a measure of the background and incoherent scattering from the sample). We might describe the observed intensity as the sum of two components: a "quasielastic" component (centered on zero energy) with a width $\hbar\Gamma \simeq 1.5$ meV and an approximately energy-independent component visible for $\hbar\omega \gtrsim 5$ meV. Following on from the analysis of the higher-energy data, we first tried to fit this data using the damped spin-wave cross section given by Eqs. (3) and (4). The inverse correlation length was chosen to be $\xi^{-1}=0.005$ Å^{-1}, the value predicted from theory[5] at this temperature and in agreement with a double-axis experiment on the same sample (see Fig. 8). The damping constant for the spin waves $\hbar\Gamma_1$ was chosen to be 3.6 meV (see below). On performing the full convolution with the instrumental resolution function [Eq. (5)], we obtain the dashed line in Fig. 7(b). We conclude that the quasielastic peak cannot be explained by (4) with the parameters we have chosen. Figure 9 shows the simulated scattered intensity $I(\omega)$ for a variety of values for the spin-wave damping $\hbar\Gamma_1$, thus demonstrating that this conclusion in unaffected by our choice for $\hbar\Gamma_1$. The dashed line in Fig. 7(b), shows that a "spin-wave" cross section, as defined by Eqs. (3) and (4), predicts a *slowly varying* scattered intensity under our experimental conditions.

We can obtain a considerably better fit to the data if we include an additional q-independent contribution to the spectral function so that (4) becomes

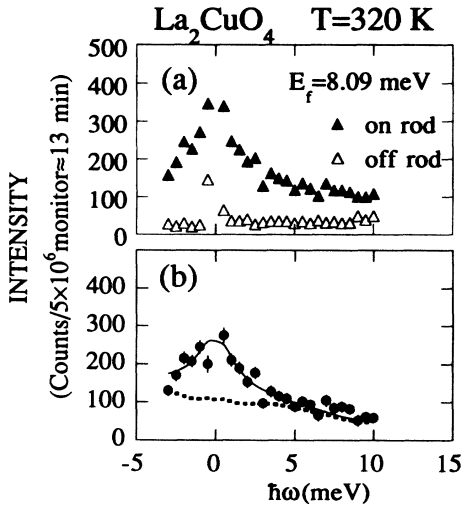

FIG. 7. (a) TAS6 (cold source, Risø) constant wave-vector scans for positions on and off the rod: Q=(1,0.52,0) and (1.06,0.52,0), respectively. The sample volume was ~1 cm^3. (b) The difference between the scans in (a) has been fitted to a cross section consisting of spin waves and a quasielastic peak as described by Eq. (6) (solid line). The dashed line represents the contribution of the spin-waves alone. Data were collected with a pyrolitic graphite (002) monochromator, a pyrolitic graphite (002) analyzer, and collimation of 90′-60′-52′-66′.

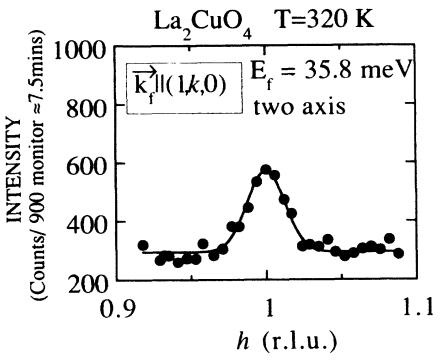

FIG. 8. A double-axis "energy-integrated" scan across the 2D rod. The direction of the outgoing neutron wave vector was arranged to be parallel to the 2D rod at each point of the scan. The ordinate refers to the elastic wave vector ($hk0$). For further details of the method see Endoh *et al.*[3] The solid line is a fit of the data to a Lorentzian convoluted with the instrumental resolution function, which yields a value for the inverse correlation length $\xi^{-1}=0.005(2)$ Å^{-1}. Data were collected with a Cu(111) monochromator and collimation of 12′-20′-10′. The sample volume was ~1 cm^3 and the instrument used was IN3 on a thermal guide at the ILL.

$$\chi''(q,\omega) = \frac{1}{(q^2+\xi^{-2})}\left(\frac{A_1\omega\Gamma_1}{\Gamma_1^2+(\omega-cq)^2} + \frac{A_1\omega\Gamma_1}{\Gamma_1^2+(\omega+cq)^2} + \frac{A_2\omega\Gamma_2}{\Gamma_2^2+\omega^2}\right), \tag{6}$$

where Γ_1 refers to the damping of the spin waves and Γ_2 to the additional q-independent contribution. The result of this analysis is shown by the solid line in Fig. 7(b), where the parameters obtained were $\hbar\Gamma_1 = 3.6\pm2.9$ meV, $\hbar\Gamma_2 = 1.5 \pm 0.4$ meV, and $A_1/A_2 = 4.9 \pm 1.4$ for T=320 K, choosing $\hbar c$=750 meV Å and $\xi^{-1}=0.005$ Å^{-1}.

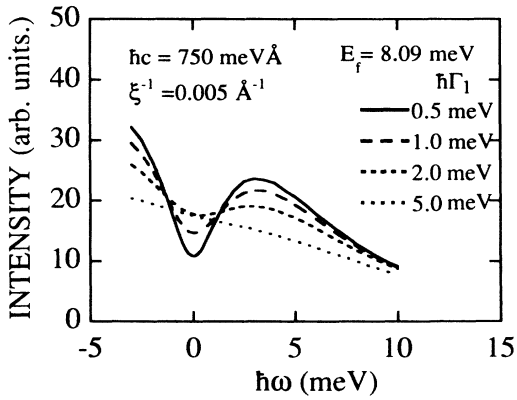

FIG. 9. Simulations of the scattered intensity (including the effects of the spectrometer resolution) for the spin-wave cross section described by Eqs. (3) and (4). The curves have been calculated numerically. The spectrometer conditions correspond to those used to collect the data in Fig. 7.

V. CONCLUSIONS

Recent calculations[9] suggest that conventional spin-wave theory should give a good description of the magnetic dynamics of La_2CuO_4 for $\hbar\omega \gtrsim kT$. It can be seen from Fig. 6 that to within the experimental error our measurements bear this out. In fact, we find that for $T \sim 300$ K, our data agree with conventional spin wave theory for $\hbar\omega \gtrsim 5$ meV $\sim \hbar c\xi^{-1}$. We can use our spin-wave velocity together with the Hamiltonian (1) to obtain an estimate for the nearest-neighbor coupling constant J. From classical spin-wave theory, the spin-wave velocity is $c = \sqrt{8}SJa$. Quantum corrections[15] for the $S = \frac{1}{2}$ case increase c by a factor of 1.18 ± 0.02, which implies that our low-temperature spin-wave velocity, $\hbar c = 0.85 \pm 0.03$ eV Å corresponds to an exchange constant of $J = 0.136 \pm 0.005$ eV. From Raman scattering[1] interpreted using spin-wave theory with quantum corrections, $J = 0.128 \pm 0.006$ eV. Thus, the error-broadened values obtained from (single-magnon) neutron scattering and two-magnon light scattering agree. Finally, we note that our analysis indicates a slight reduction in the spin-wave velocity from 0.85 ± 0.03 to 0.75 ± 0.03 eV Å on raising T from 5 to 300 K.

We now turn to the lower-energy results. The dynamics of the quantum 2D Heisenberg antiferromagnet have been investigated theoretically using a number of techniques. In the regime $\hbar\omega \lesssim \hbar c\xi^{-1}$, spin-wave interactions are the main mechanism for damping. Grempel[11] estimated the order-parameter relaxation rate for $q=0$ using a coupled-mode calculation and found that $\hbar\Gamma_2 \simeq \hbar c\xi^{-1}(T/2\pi\rho_s)^{\frac{1}{2}}$. Tyč, Halperin, and Chakravarty[12] used numerical simulation supplemented by dynamic-scaling considerations to predict $\chi(q,\omega)$. Their prediction for $\hbar\Gamma_2$ is in agreement with that of Grempel. We do not attempt here a detailed comparison with the simulated $\chi(q,\omega)$, since our q resolution is relatively poor. However, we can compare the theoretical and experimental results for $\hbar\Gamma_2$. Using Grempel's formula with the values $\rho_s \simeq 0.15J$, J=0.13 eV, and ξ^{-1}=0.005 Å^{-1} appropriate for our experiment at T=320 K, we obtain $\hbar\Gamma_2$=1.7 meV, in good agreement with the value obtained directly from the measurements described in Sec. III.

In summary, we have measured the magnetic dynamics of La_2CuO_4 over the energy range $0 \leq \hbar\omega \leq 140$ meV. In both the antiferromagnetic as well as the paramagnetic phases, we find that conventional spin wave theory gives an excellent account of the data with $\hbar\omega \gtrsim \hbar c\xi^{-1}$. In other words, classical theory yields the observed forms for not only the dispersion relation but also the spin-wave amplitudes.

ACKNOWLEDGMENTS

We are grateful to D. Grempel and R. Singh for helpful discussions of their theoretical ideas. Two of us (S.M.H. and G.A.) thank the staff at Risø National Laboratory for its hospitality and support during the low-energy experiments reported here. We are especially grateful to M. Nielsen and K. Clausen for practical assistance and advice.

---

*Also at Risø National Laboratory, DK-4000, Roskilde, Denmark.

†Present address: AT&T Bell Laboratories, Murray Hill, New Jersey 07974.

[1] K. Lyons, P. A. Fleury, J. P. Remeika, A. S. Cooper, and T. J. Negran, Phys. Rev. B **37**, 2353 (1988); R. R. P. Singh, P. A. Fleury, K. B. Lyons, and P. E. Sulewski, Phys. Rev. Lett. **62**, 2736 (1989).

[2] D. Harshman *et al.*, Phys. Rev. B **38**, 852 (1988); J. Budnick *et al.*, Europhys. Lett. **5**, 651 (1988); Y. Uemura *et al.*, Phys. Rev. Lett. **59**, 1045 (1987).

[3] Y. Endoh, K. Yamada, R.J. Bigeneau, D. R. Gabbe, H.P. Jenssen, M.A. Kastner, C.J. Peters, P.J. Picone, T.R. Thurston, J.M. Tranquada, G. Shirane, Y. Hidaka, M. Oda, Y. Enomoto, M. Suzuki, and T. Murakami, Phys. Rev. B **37**, 7443 (1988).

[4] K.Yamada, K. Kakurai, Y. Endoh, T.R. Thurston, M.A. Kastner, R.J. Birgeneau, G. Shirane, Y. Hidaka, and T. Murakami, Phys. Rev. B **40**, 4557 (1989).

[5] S. Chakravarty, B.I. Halperin, and D.R. Nelson, Phys. Rev. Lett. **60**, 1057 (1988); Phys. Rev. B **39**, 2344 (1989).

[6] S-W. Cheong, J.D. Thompson, and Z. Fisk, Phys. Rev. B **39**, 4395 (1989).

[7] G. Shirane, Y. Endoh, R.J. Birgeneau, M.A. Kastner, Y. Hidaka, M. Oda, Y. Enomoto, M. Suzuki, and T. Murakami, Phys. Rev. Lett. **59**, 1613 (1987).

[8] G. Aeppli, S.M. Hayden, H.A. Mook, Z. Fisk, S-W. Cheong, D. Rytz, J.P. Remeika, G.P. Espinosa, and A.S. Cooper, Phys. Rev. Lett. **62**, 2052 (1989).

[9] D.R. Grempel, in *New Tends in Magnetism*, edited by S. Rezende and M. Coutinho-Filho (North-Holland, Amsterdam, 1990).

[10] See, for example, S.W. Lovesey, *Theory of Neutron Scattering from Condensed Matter* (Oxford University Press, Oxford, 1984). By "conventional" here we mean that the ground state is taken to be the Néel state.

[11] D.R. Grempel, Phys. Rev. Lett. **61**, 1041 (1988).

[12] Stéphane Tyč, Bertrand I. Halperin, and Sudip Chakravarty, Phys. Rev. Lett. **62**, 835 (1989).

[13] B. Dorner, Acta Crystallogr. A **28**, 319 (1972).

[14] M. J. Cooper and R. Nathans, Acta Crystallogr. **23**, 357 (1967).

[15] R.R.P. Singh, Phys Rev. B **39**, 9760 (1989).

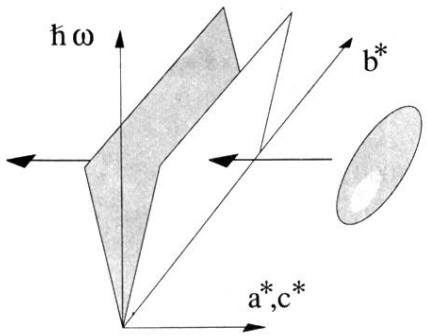

FIG. 3. Illustrates how constant energy scans were made through the spin-wave dispersion surface. The ellipsoid represents the instrumental resolution.